Free carrier induced spectral shift for GaAs filled metallic hole arrays

Jingyu Zhang[1,2,*], Bin Xiang[3], Mansoor Sheik-Bahae[4], and S. R. J. Brueck[1]

[1] *Center for High Technology Materials and Department of Electrical and Computer Engineering, University of New Mexico, 1313 Goddard SE, Albuquerque, New Mexico 87106, USA*

[2] *Current address: Sharp Laboratories of America, 5750 NW Pacific Rim Blvd, Camas, Washington 98607, USA*

[3] *National Center for Electron Microscopy, Lawrence Berkeley National Laboratory, Berkeley, California 94720, USA*

[4] *Department of Physics and Astronomy, University of New Mexico, 800 Yale Boulevard NE, Albuquerque, New Mexico 87131, USA*

[*] *Jingyuzhang3@gmail.com*

Abstract: For a GaAs filled metallic hole array on a pre-epi GaAs substrate, the free carriers, generated by three-photon absorption (3PA) assisted by strongly enhanced local fields, reduce the refractive index of GaAs in ~200-nm thick active area through band filling and free carrier absorption. Therefore, the surface plasma wave (SPW) resonance, and the related second harmonic (SH) spectrum blue shifts with increasing fluence; For the plasmonic structure on a substrate with surface defects, free carrier recombination dominates. The band gap emission spectral peak wavelength decreases 10-nm with increasing fluence, showing the transition from nonradiative-, at low excitation, to bimolecular-recombination at high carrier concentrations.

OCIS codes: (310.6628) Subwavelength structures;(190.4350) Nonlinear optics at surfaces

References and links

1. J. M. Luther, P. K. I. Jain, T. Ewers, and A. P. Alivisatos, "Localized surface plasmon resonances arising from free carriers in doped quantum dots," Nat. Mater. **10**(5), 361–366 (2011).
2. W. Fan, S. Zhang, B. Minhas, K. J. Malloy, and S. R. J. Brueck, "Enhanced infrared transmission through subwavelength coaxial metallic arrays," Phys. Rev. Lett. **94**(3), 033902 (2005).
3. J. Zhang, S. Zhang, D. Li, A. Neumann, C. Hains, A. Frauenglass, and S. R. J. Brueck, "Infrared transmission resonances in double layered, complementary-structure metallic Gratings," Opt. Express **15**, 8737–8744 (2007).
4. W. Fan, S. Zhang, N.-C. Panoiu, A. Abdenour, S. Krishna, R. M. Osgood, Jr., K. J. Malloy, and S. R. J. Brueck, "Second harmonic generation from a nanopatterned isotropic nonlinear material," Nano Lett. **6**(5), 1027–1030 (2006).
5. K. Chen, C. Durak, J. R. Heflin, and H. D. Robinson, "Plasmon-enhanced second-harmonic generation from ionic self-assembled multilayer films," Nano Lett. **7**(2), 254–258 (2007).
6. F. B. P. Niesler, N. Feth, S. Linden, J. Niegemann, J. Gieseler, K. Busch, and M. Wegener, "Second-harmonic generation from split-ring resonators on a GaAs substrate," Opt. Lett. **34**(13), 1997–1999 (2009).
7. J. Butet, J. Duboisset, G. Bachelier, I. Russier-Antoine, E. Benichou, C. Jonin, and P. F. Brevet, "Optical second harmonic generation of single metallic nanoparticles embedded in a homogeneous medium," Nano Lett. **10**(5), 1717–1721 (2010).
8. Y. Zhang, N. K. Grady, C. Ayala-Orozco, and N. J. Halas, "Three-dimensional nanostructures as highly efficient generators of second harmonic light," Nano Lett. **11**(12), 5519–5523 (2011).
9. W. Cai, A. P. Vasudev, and M. L. Brongersma, "Electrically controlled nonlinear generation of light with plasmonics," Science **333**(6050), 1720–1723 (2011).
10. J. Zhang, L. Wang, S. Krishna, M. Sheik-Bahae, and S. R. J. Brueck, "Saturation of the second harmonic generation from GaAs filled metallic hole arrays by nonlinear absorption," Phys. Rev. B **83**(16), 165438 (2011).
11. R. H. Ritchie, "Plasma loss by fast electrons in thin films," Phys. Rev. **106**(5), 874–881 (1957).
12. B. R. Bennett, R. A. Soref, and J. A. D. Alamo, "Carrier-induced change in refractive index of InP, GaAs, and InGaAsP," IEEE J. Quantum Electron. **26**(1), 113–122 (1990).
13. J. Zhang and S. R. J. Brueck, "Multi-photon absorption and second harmonic generation in GaAs-Filled Nanoplasmonic Arrays," in *Asia Communications and Photonics Conference and Exhibition (ACP)(Academic,*Shanghai, China, 2009)
14. J. Zhang, "Metallic photonic crystals: transmission resonance and second harmonic generation," (Ph. D thesis of University of New Mexico, 2009), Chap. 4. *http://repository.unm.edu/handle/1928/10357*

#162001 - $15.00 USD Received 23 Jan 2012; revised 28 Feb 2012; accepted 4 Mar 2012; published 13 Mar 2012

15. R. Schroeder and B. Ullrich, "Absorption and subsequent emission saturation of two-photon excited materials: theory and experiment," Opt. Lett. **27**(15), 1285–1287 (2002).
16. J. U. Kang, A. Villeneuve, M. Sheik-Bahae, G. I. Stegeman, K. Al-hemyari, J. S. Aitchison, and C. N. Ironside, "Limitation due to three-photon absorption on the useful spectral range for nonlinear optics in AlGaAs below half band gap," Appl. Phys. Lett. **65**(2), 147 (1994).
17. W. C. Hurlbut, Y.-S. Lee, K. L. Vodopyanov, P. S. Kuo, and M. M. Fejer, "Multiphoton absorption and nonlinear refraction of GaAs in the mid-infrared," Opt. Lett. **32**(6), 668–670 (2007).
18. M. P. Hasselbeck, E. W. Van Stryland, and M. Sheik-Bahae, "Scaling of four-photon absorption in InAs," J. Opt. Soc. Am. B **14**(7), 1616–1624 (1997).
19. R. Braunstein and E. O. Kane, "Valance band structure of III-V compounds," J. Phys. Chem. Solids **23**(10), 1423–1431 (1962).
20. L. D. Landau and E. M. Lifshitz, Electrodynamics of Continuous Media (Addison-Wesley, Reading, Mass., 1960), p. 260.
21. C. H. Henry, R. A. Logan, and K. A. Bertness, "Spectral dependence of the change in refractive index due to carrier injection in GaAs lasers," J. Appl. Phys. **52**(7), 4457–4461 (1981).

1. Introduction

The interaction of nanoscale metals with light is characterized by surface-bound charge density oscillations of their free electrons in resonance with the driving electromagnetic field [1]. The coupling of the surface plasmon waves (SPWs) with local cavity resonances strongly enhances local electromagnetic fields [2,3]. Most reports have concentrated on the nonlinear second harmonic generation as a function of intensity [4–9]; additionally there are shifts from local field enhanced plasmonic structure. However, the SHG intensity or conversion efficiency is very low for real applications due to the nanoscale active volume. The reported highest conversion efficiency is still less than 10^{-5} [10]. As described in our previous paper [10], free carriers N_e, generated by three photon absorption associated with the enhanced local field intensity in the plasmonic structure, attenuates the SHG. Thus, the conversion efficiency is limited even with high pump intensity. Here, we report a SH spectral shift with increasing fluence, which reflects the local carrier concentration variation under optical excitation. At room temperature (297K), with increasing fluence at a GW/cm^2 scale, the spectral peak and linewidth variation of the second harmonic generation (SHG) and bandgap emission (BE, photoluminescence PL) from GaAs filled metallic hole arrays follows the trends of their intensity. The high concentration of free carriers N_e, not only attenuates the fundamental intensity, but also affects the dielectric constant of GaAs $\varepsilon(\omega)$ [10], through a Drude interaction [11]. The dielectric constant decreases ($\Delta n < 0$) with increasing fluence due to bandfilling and free carrier absorption [12]. The SPW resonance frequency, given approximately by a simple kinetic model (momentum conservation) [2,3] blueshifts with the decreasing dielectric constant. Therefore, the fundamental near-infrared output spectrum, resulting from the first order transmission spectrum of the plasmonic structure [13], is reshaped and shifted [14], confirming the free carrier induced SHG spectral shifting. Compared with the SHG spectral shifting from the GaAs filled metallic structure, the SHG spectral peak from a bare GaAs substrate is constant at half of fundamental wavelength with the same input peak power. The result confirms that free carriers generated by multi-photon absorption associated with the local enhanced fields in the plasmonic structure affect the dielectric constant and the resulting SHG spectrum.

When the plasmonic sample is thinned by back-side etching, surface defects are introduced. Free carrier recombination dominates at room temperature. The SHG spectrum shifts slightly but the PL spectrum shifts more dramatically, by about 15 nm with increasing fluence, due to the transition from nonradiative carrier recombination at low excitation to bimolecular radiative recombination at high carrier concentration. When the sample is cooled down to 77K, the SHG and BE spectra exhibit constant peak wavelengths with narrowed linewidths.

The sample is fabricated on a double polished pre-epi GaAs substrate with GaAs posts (110-nm height) extending through holes in Au film arrays (540-nm pitch; 220-nm diameter, 100-nm height). The fabrication flow and structure have been described in Ref [10]. The linear spectrum is measured by Fourier transform infrared spectroscopy (FTIR). The first order SPW coupling (observed as a transmission dip) is at 1880-nm and the coupled first

#162001 - $15.00 USD Received 23 Jan 2012; revised 28 Feb 2012; accepted 4 Mar 2012; published 13 Mar 2012

order transmission peak is at 2190-nm [13, 14]. The unit cell includes one GaAs post. By using a near infrared (~2090-nm) fundamental wavelength at normal incidence, the SPWs are coupled into local modes with strongest enhanced electric fields E_x and E_z, which give the dominant contribution to the SHG, as shown in Ref [10], as a result of the $\bar{4}3m$ GaAs crystal point group

We exploited the measurement setup described in Ref [10]. A pulsed laser with 200 fs pulse duration and 1 kHz repetition rate with a tunable wavelength is focused to the backside of the test sample at normal incidence. The fundamental laser pulse is 70-nm linewidth at near-infrared (NIR). The sample is located in a Dewar for ambient temperature control. Both the band gap photoluminescence (BE) and the second-harmonic radiation are collected and focused to a monochrometer and InGaAs detector with a scanning wavelength from 800- to 1700-nm.

2. Free carrier refraction from plasmon-coupled hole arrays on a pre-epi GaAs substrate at 297K

The SHG signal is monitored as the incident wavelength is tuned from 1900- to 2200 nm across the fundamental SPW resonance at different fluences. The SH signal around 1045-nm wavelength and BE signal at 890-nm wavelength are monitored as a function of the fundamental fluence. As shown in Fig. 1, with the increase of fundamental intensity, no dramatic shift is observed in the BE spectrum, while the SHG spectrum blueshifts from 1045 to 1020-nm as the fluence is increase from 7- to 127-GW/cm^2.

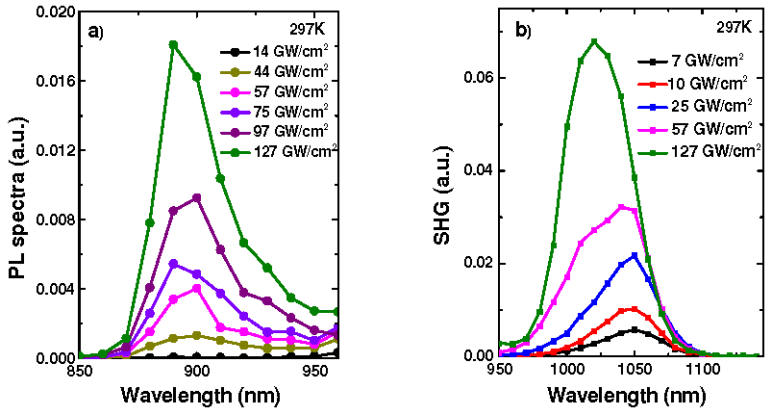

Fig. 1. At 297K, for the plasmonic structure on a 500μm double polished pre-epi GaAs substrate, (a) BE (PL) spectral peak only slightly shifts (~890 nm); (b) SH spectral peak blueshifts from 1045 to 1023-nm with increasing fluencies from 7- to 127-GW/cm^2.

The output response of SHG and BE is spectrally integrated and plotted versus the 2090-nm fundamental intensity (input pulse peak power) as shown in the Fig. 5 in Ref [10]. At 297K, for the GaAs substrate at low input peak power <10 GW/cm^2, no SH signal was observed. A weak SH signal was observed at higher input peak powers with a slope of 1.1 due to weak focusing. The BE signal increases as the third power of the fundamental fluence. At 297K, for the plasmon coupled hole arrays, the SHG exhibits the expected quadratic power law dependence $I_{2\omega} \propto I_{\omega}^2$ at low input power (< 10 GW/cm^2), then saturates, with two orders enhancement compared with that of bulk GaAs. The BE signal appears at incident intensities coincident with the saturation of the SHG with a slope of 2.8. The free carrier generation across the GaAs bandgap is excited by 3PA at the fundamental frequency [10].

#162001 - $15.00 USD Received 23 Jan 2012; revised 28 Feb 2012; accepted 4 Mar 2012; published 13 Mar 2012

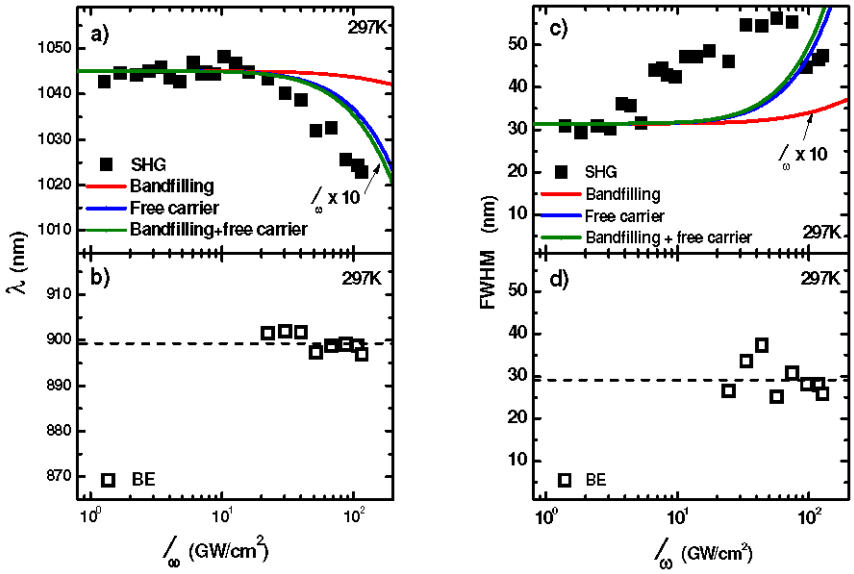

Fig. 2. At 297K, for the plasmon-coupled structure on a double polished 500 μm thick double polished pre-epi GaAs substrate, the spectral peak and linewidth (measured in squares and simulated in solid line) variation with increasing fluences: (a) SHG spectral peaks blueshift from 1045- to 1023-nm shows strong refractive index changes due to bandfilling (in red) and free carrier absorption (FCA) (in blue) and the combined effects (bandfilling and FCA in green); (b) BE spectral peak wavelength (PL) shows 3PA generated carriers recombination without obvious spectral shifting; (c) Linewidth of SHG spectra are broadened from 30- to 58-nm, evidencing the negative Δn with increasing fluences; (d) the linewidth of BE spectrum does not show obvious linewidth broadening.

At room temperature, for the plasmonic structure on a pre-epi GaAs substrate, the spectral peak wavelength and the full width half maximum (FWHM, linewidth) of SHG and BE with fundamental intensity in linear-log coordination have been plotted in Fig. 2. The SHG peak wavelength is constant at 1045-nm with input peak power from 1 to 10-GW/cm^2, and then blue shifts from 1045- to 1023-nm with the input peak power from 10 to 100-GW/cm^2 as shown in Fig. 2(a). The BE spectral peak is relatively constant with increasing fluences, as shown in Fig. 2(b). The linewidth of SHG spectrum is broadened from 30 nm to 58 nm with increasing fluence, as shown in Fig. 2(c). The linewidth of BE spectrum is relatively constant with increasing fluence, as shown in Fig. 2(d). The trend of wavelength shift of SHG peak with increasing input peak power is consistent with that of the intensity of SHG with increasing input peak power as the Fig. 5 in Ref [10]. However, for a bulk GaAs substrate at the same temperature, the wavelength peak of SHG and PL are constant at 1050/1040nm and 890/900nm. Therefore, the free carriers generated by the nonlinear 3PA, associated with the enhanced localized electric field with an four orders enhanced coefficient of 3PA from each unit cell [4], introduces a refractive index change and a consequent spectral shift.

We assume the input pulse has a Gaussian temporal shape with FWHM τ (200 fs) $I_\omega(t) = I_0 \exp\left[-4\ln(2)\frac{t^2}{\tau^2}\right]$ [15]. The generated carriers, $N_e = N_h$, are excited from 3PA of $\hbar\omega$ (1.78 eV), as expressed in Eq. (1), is proportional to I_ω^3, where I_ω is the laser irradiance (W/cm^2). The carrier concentration is ~10^{20} cm^{-3} resulting from 3PA of $3\hbar\omega$ (1.78 eV) with ~100 GW/cm^2 input peak power. The coefficient of 3PA ρ^{3PA} is 3.8 × 10^4 from each unit cell at the concentration [10]. The nonlinear absorption coefficient of 3PA K^{3PA} is 3 × 10^{-19} cm^3/W^2 [16,17]. The second term on the right-hand side of Eq. (1) is set to zero for calculating the carrier concentration during the laser pulse, given no recombination during the

#162001 - $15.00 USD Received 23 Jan 2012; revised 28 Feb 2012; accepted 4 Mar 2012; published 13 Mar 2012

laser pulse. The rate equation for the depletion of the fundamental intensity caused by 3PA and FCA is given in Eq. (2) [18]. The refractive index n_ω is 3.34. The irradiance independent hole cross section is $\sigma_H = 1 \times 10^{-16}$ cm^2 [19].

$$\frac{dN_e}{dt} = \rho^{3PA} \frac{K^{3PA}(\omega,\omega,\omega)}{3\hbar\omega} I_\omega^3 - \frac{N_e}{T_1} \tag{1}$$

$$\frac{n_\omega}{c}\frac{\partial}{\partial t} I_\omega(t) = -\rho^{3PA} K^{3PA}(\omega,\omega,\omega) I_\omega^3 - \sigma_h(\omega) N_e I_\omega \tag{2 [13]}$$

$$\Delta n_{bandfilling}(N_e,\omega) = \frac{cP}{\pi}\int_0^\infty \frac{\alpha(N_e,\omega') - \alpha(0,\omega')}{\omega'^2 - \omega^2} d\omega' \tag{3 [9]}$$

$$\Delta n_{freecarrier}(N_e,\omega) = -\left(\frac{e^2\lambda^2}{8\pi^2 c^2 \varepsilon_0 n_\omega}\right)\left(\frac{N_e}{m_e} + N_h\left(\frac{m_{hh}^{1/2} + m_{lh}^{1/2}}{m_{hh}^{3/2} + m_{lh}^{3/2}}\right)\right) \tag{4 [9]}$$

$$n(N_e,\omega) = n_0(\omega) + \Delta n_{bandfilling}(N_e,\omega) + \Delta n_{freecarrier}(N_e,\omega) \tag{5}$$

$$\lambda_{SPW}(N_e) = \frac{\Lambda}{m}\left(\mathrm{Re}\sqrt{\frac{n(N_e,\omega)^2 \varepsilon_m}{n(N_e,\omega)^2 + \varepsilon_m}} \pm \sin\theta\right) \tag{6 [2]}$$

$$\Delta\omega = -\frac{\partial\phi}{\partial t} = -\frac{\omega L}{c}\frac{\partial n}{\partial t} \approx -\frac{\omega L}{c}\frac{\Delta n}{t_p} \tag{7}$$

The high carrier concentration contributes refractive index change due to bandfilling and free carrier absorption (FCA). With the lowest energy states in the conduction band filled, electrons from the valence band require energies greater than the nominal bandgap to be optically excited into the conduction band through 3PA. Hence, there is a decrease in the absorption coefficient $\alpha(\omega, N_e)$ at energies above the band gap [12]. The refractive index change $\Delta n_{bandfilling}(N_e, 2\omega)$, due to free carrier band filling caused by the decease of the absorption coefficient, is expressed as Eq. (3), where P indicates the principal value of the integral [20]. For intrinsic GaAs bulk, the absorption coefficient $\alpha(0,\omega) = \frac{C_{hh}}{\omega}\sqrt{\omega - \omega_g} + \frac{C_{lh}}{\omega}\sqrt{\omega - \omega_g}$, at $\omega \geq \omega_g$; and $\alpha(0,\omega) = 0$ at $\omega < \omega_g$. ω_g is the bad-gap frequency. C_{hh} and C_{hh} refer to heavy and light holes, respectively. $C_{hh} = 1.5\times10^{12} cm^{-1}\cdot s^{-1/2}$, and $C_{lh} = 7.8\times10^{11} cm^{-1}\cdot s^{-1/2}$ for GaAs [12]. When the conduction band is filled with electrons, the absorption coefficient is expressed as $\alpha(N_e,\omega) = \alpha_0(\omega)\cdot\left[f_v(E_a) - f_c(E_b)\right]$ [12]. $f_v(E_a)$ is the probability of a valence band state of energy E_a being occupied by an electron and $f_c(E_b)$ is the probability of a conduction band state of energy E_b being occupied by an electron. The detailed derivation of Eq. (3) is referred in Ref [12].

The refractive index change associated with the free carriers, $\Delta n_{freecarrier}(N_e,\omega)$, is directly proportional to the concentration of electrons and holes and inversely proportional to the square of the photon energy ($\hbar\omega$), as expressed in Eq. (4). m_e, m_{lh}, m_{hh} are the mass of electrons, heavy holes and light holes. $m_e = 0.066 m_0$, $m_{hh} = 0.45 m_0$, $m_{lh} = 0.084 m_0$, $m_0 = 9.11\times10^{-31} kg$, is the free electron rest mass. The parameters for GaAs were listed in Ref [12,21].

#162001 - $15.00 USD Received 23 Jan 2012; revised 28 Feb 2012; accepted 4 Mar 2012; published 13 Mar 2012

The total index change (Eq. (5)) will introduce the wavelength shift of SPWs. The kinetic model is expressed in the Eq. (6). The shift of linear transmission peak due to the index change is approximately that of the SPW resonance [2,3]. The linewidth of linear transmission spectrum (ranging from 1.9 to 2.7-μm) coupled by the first order SPWs is ~500 nm [10]. The input Gaussian shaped laser pulse at the fundamental wavelength (2.09 μm) with ~70 nm linewidth is within the linear transmission spectrum of the plasmonic structure [14]. The shift of the linear spectrum will reshape the input laser pulse. The wavelength of pulse peak will shift with the linear transmission spectrum. The spectral peak of $\lambda_{SHG} = \lambda_{fundamental} / 2$ is plotted in Fig. 4(a) with index changed by band filling (in red) and FCA (in blue). The SHG shift due to the index change resulting from FCA is significant compared with that resulting from band filling. The fundamental intensity is magnified to the order of 10x in simulation for comparing experiment data. The difference of fundamental intensity between experiment and simulation may be due to the inaccuracy of nonlinear coefficiencies and scattering loss in instrument during measurement [10].

The frequency linewidth due to index change, as expressed as Eq. (7), is converted to wavelength linewidth of index change $\frac{\Delta\lambda}{\lambda} \approx -\frac{L}{c}\frac{\Delta n}{t_p} \approx -\Delta n$ with $L \approx c \cdot t_p$, where t_p is the time for a pulse passing through the active layer of GaAs (~100nm) [10]. Therefore, the linewidth of the SHG spectrum is broaden with the $\Delta n(<0)$ decrease under increasing fluences. The index decrease is resulted from high free carrier concentration pumped by increased input peak power. The broaden linewidth of SHG from Eq. (7) fits the experimental data trend as shown in Fig. 4(c).

3. Carrier recombination from plasmon-coupled hole arrays on a 20 μm wet etched GaAs substrate at 297K

A ~2 mm diameter hole was etched from back side of the sample by using a solution of H_2SO_4: H_2O_2: H_2O (1:8:1). The remaining GaAs substrate under the plasmonic structure was ~20 μm thick with a mirror like etched surface full of submicron scale porous and particles. The serious surface defects are likely to be damage to the GaAs giving rise to a decrease in nonradiative recombination time τ_{NR} compared to bulk material [10].

The line-width integrated BE and SH intensities versus fundamental intensity are plotted in Fig. 3 in a log-log coordination. At 297 K, the SHG saturates at the same threshold input peak power, ~10 GW/cm^2, as that for the plasmon-coupled structure on pre-epi GaAs substrate. However, the PL intensity shows a trend from 3rd, to 9th, and back to 3rd order dependence on the incident fluence. The BE intensity shows $I_{BE} \propto I_{\omega}^{2.5}$ at fundamental power from 10 to 25-GW/cm^2. It is then strongly enhanced at fundamental power from 25 to 40-GW/cm^2 with 9th order fundamental intensity dependence, compared with the signal from the plasmon-coupled structure on the pre-epi GaAs substrate with 3rd order fundamental intensity dependence, even under 3PA excitation [10]. The BE power scales back as $I_{BE} \propto I_{\omega}^{2.6}$ at the input peak power higher than 40 GW/cm^2. The trend of BE intensity vs. input peak power, as been done in Ref [10], is due to the transition from nonradiative to bimolecular radiative-dominated carrier recombination. The radiative recombination carrier density vs. input peak power with τ_{NR} = 0.1 ns, simulated and plotted in Fig. 3(b), as done in Ref [10], shows the transition from nonradiative at low excitation to bimolecular recombination at high carrier concentrations. The model explained the experimental data clearly.

#162001 - $15.00 USD Received 23 Jan 2012; revised 28 Feb 2012; accepted 4 Mar 2012; published 13 Mar 2012

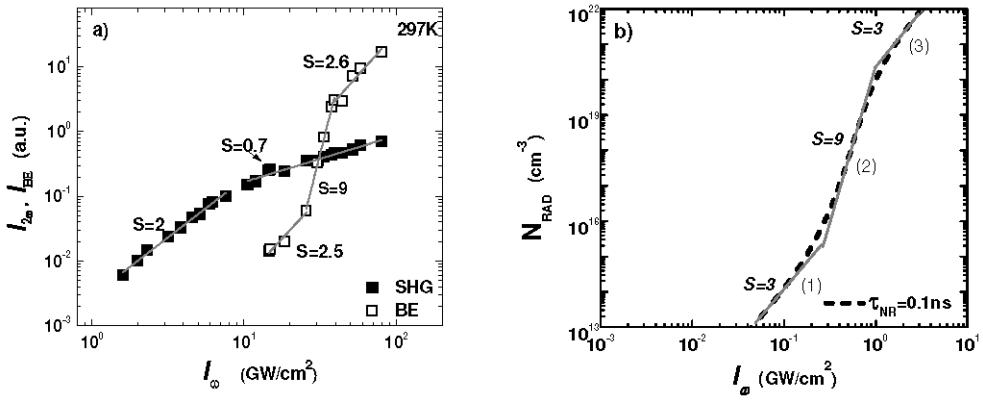

Fig. 3. (a) At 297K, for the plasmon-coupled structure on a 20 μm wet etched GaAs substrate with surface defects, SHG intensity (solid square) $I_{2\omega} \propto I_\omega^2$ at input peak power < 10 GW/cm^2, and then $I_{2\omega} \propto I_\omega^{0.7}$ at input peak power > 10 GW/cm^2; The BE intensity (unfilled square) showed $I_{BE} \propto I_\omega^{2.5}$at input peak power from 10- to 25 GW/cm^2, $I_{BE} \propto I_\omega^{9}$ at input peak powers from 25- to 40 GW/cm^2, and $I_{BE} \propto I_\omega^{2.6}$at fundamental power > 40 GW/cm^2. (b) The simulated radiative recombination carrier density vs. input peak power with τ_{NR} = 0.1 ns in log-log plot.

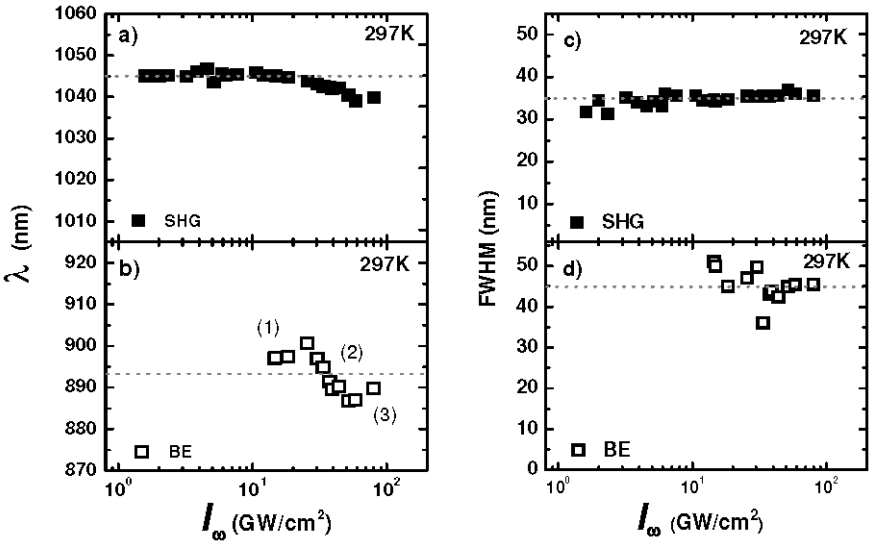

Fig. 4. At 297K, for the plasmon-coupled structure on a 20 μm thick GaAs substrate with surface defects by wet etching, the spectral variation of SHG and BE vs the increasing fluences in linear-log plots: (a) SHG spectrum is constant at 1045-nm with 2090-nm fundamental wavelength at low irradiance (1- to 10-GW/cm^2) and shows minor refractive index changes (5-nm) at high irradiance (10- to 100-GW/cm^2) and (b) BE (PL) spectrum wavelength shows optical frequency switch from 900- to 887-nm with increase of fluence from 25 to 50 GW/cm^2. (c) Linewidths of the SHG spectra are unchanged from 1- to 100-GW/cm^2; (d) the BE spectrum shows an averaged 45nm linewidth.

The SHG spectrum peaks and BE spectrum peaks wavelength vs input peak power were plotted in linear-log plots in Fig. 4*s*. As shown in Fig. 4(a), the SHG spectral wavelength is constant at fluences from 1- to 10-GW/cm^2, and then blue shifts slightly at fluences from 10- to 100-GW/cm^2 due to the band filling induced refractive index change, as simulated in Fig. 2(a). In Fig. 4(b), the wavelength of PL peaks shows switch trend which consists with trend of the BE intensity dependence of fluences as shown in Fig. 3(a). The PL happens at ~900-nm at low fluences (10- to 25- GW/cm^2), blueshifts to 887-nm rapidly with input peak power > 50-

#162001 - $15.00 USD Received 23 Jan 2012; revised 28 Feb 2012; accepted 4 Mar 2012; published 13 Mar 2012

GW/cm^2. The linewidth of SHG, as shown in Fig. 4(c) is constant with increasing peak power due to slightly varied refractive index compared with the plasmonic structure on pre-epi GaAs substrate. The linewidth of PL is as broad as 45-nm in Fig. 4(d) due to the surface state density.

4. Carrier recombination from plasmon-coupled hole arrays on a 20 μm wet etched GaAs substrate at 77K

For the plasmonic structure on 20 μm wet etched GaAs substrate, when the sample is cooled down to 77K, the SHG spectral peak and BE spectral peak are constant with increasing input peak power as shown in Fig. 5(a) and 5(b). The temperature dependent PL wavelength blue shifts to 827 nm (77K), following $E_g(T) = 1.519 - 5.41 \cdot T^2/(T + 204)$ in eV for GaAs. The FWHM of SHG and BE spectra are constant at 20- and 10-nm with increasing input peak power as shown in Fig. 5(c) and 5(d), respectively. The reduced linewidth of SHG and BE is due to the decrease of the nonradiative radiation and defects scattering at low temperature.

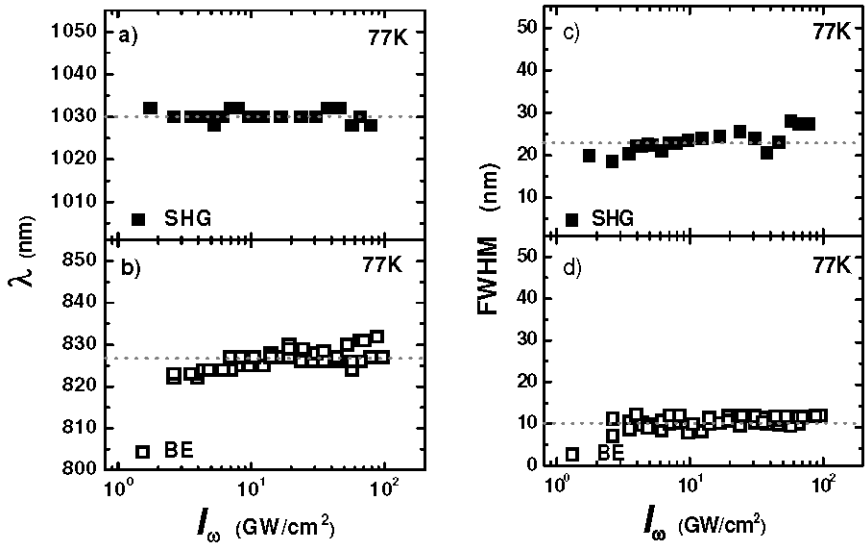

Fig. 5. At 77K, for the plasmon-coupled structure on a 20 μm thick GaAs substrate with surface defects by acid etching, the spectral variation of SHG and BE vs fundamental intensity in linear-log plots: (a) SHG spectrum keeps constant at 1030-nm with 2060-nm fundamental wavelength and (b) BE spectrum wavelength shows constant at ~827-nm with increasing fluences. Linewidth of SHG spectra (c) and BE spectra (d) are constant at 20- and 10-nm with increasing input peak power respectively.

5. Conclusion

GaAs filled subwavelength metallic hole arrays on a pre-epi GaAs substrate, pumped with a fs-duration near-infrared wavelength laser at 297K, produces SHG that saturates as a result of three-photon band-to-band and free carrier intraband absorption. Free carriers, excited by 3PA with the coefficient of 3PA ρ^{3PA} = 3.8 × 10^4 from each unit cell due to local field enhancement, induce refractive index change at high carrier concentration (10^{20}/cm^2) which blue shifts and broadens the SHG resonance linewidth. The subwavelength periodic structure on a wet etched thin GaAs substrate with surface defects shows carrier recombination emission that shifts with excitation from low frequency (902-nm) to high frequency (886-nm) with fluences from 25- to 50-GW/cm^2 at 297K, resulting from a transition from nonradiative carrier recombination at the defected GaAs surface at low excitation to bimolecular recombination at high carrier concentrations.

#162001 - $15.00 USD Received 23 Jan 2012; revised 28 Feb 2012; accepted 4 Mar 2012; published 13 Mar 2012

Acknowledgments

This work was supported by the National Science Foundation under Grant 0515684 and by the ARO under a subcontract from Redondo Optics, Inc.

#162001 - $15.00 USD Received 23 Jan 2012; revised 28 Feb 2012; accepted 4 Mar 2012; published 13 Mar 2012